chemosensors

MDPI

Review

Chemical Vapour Deposition of Gas Sensitive Metal Oxides

Stella Vallejos [1], Francesco Di Maggio [2], Tahira Shujah [3] and Chris Blackman [2,*]

1 SIX Research Centre, Brno University of Technology, Technická 10, Brno, CZ-61600, Czech Republic; vargas@feec.vutbr.cz

2 Department of Chemistry, University College London, 20 Gordon Street, London, WC1H 0AJ, UK; Francesco.dimaggio.12@ucl.ac.uk

3 Material Science and Nanotechnology Lab, Department of Physics, GC University Lahore, Pakistan; tahira_gcu@hotmail.com

* Correspondence: c.blackman@ucl.ac.uk; Tel.: +44-208-7679-4703; Fax: +44-208-7679-7463

Academic Editor: Russell Binions

Received: 17 November 2015; Accepted: 5 February 2016; Published: 1 March 2016

Abstract: This article presents a review of recent research efforts and developments for the fabrication of metal-oxide gas sensors using chemical vapour deposition (CVD), presenting its potential advantages as a materials synthesis technique for gas sensors along with a discussion of their sensing performance. Thin films typically have poorer gas sensing performance compared to traditional screen printed equivalents, attributed to reduced porosity, but the ability to integrate materials directly with the sensor platform provides important process benefits compared to competing synthetic techniques. We conclude that these advantages are likely to drive increased interest in the use of CVD for gas sensor materials over the next decade, whilst the ability to manipulate deposition conditions to alter microstructure can help mitigate the potentially reduced performance in thin films, hence the current prospects for use of CVD in this field look excellent.

Keywords: metal oxide; sensor; nano; chemical vapor deposition; CVD

1. Introduction

Gas detection, and determining the composition of gas mixtures, is necessary in many different fields, for example environmental monitoring, vehicle and industrial emission control and household security. Most studies have focused on the detection of H_2, CO_2, CO, O_2, O_3 or NH_3, because of their toxicity, their relation with atmospheric composition or the fact that they can be found at high levels in some environments. Detection of organic vapors such as methanol, ethanol, isopropanol, benzene and amines are also of great interest [1]. Metal oxides were some of the first materials used in chemoresistive gas sensors and are still the most widely used gas sensing materials. Numerous metal oxide semiconductor materials, including both single (e.g., ZnO, SnO_2, WO_3, TiO_2 and Fe_2O_3) and multi-component ($BiFeO_3$, $MgAl_2O_4$, $SrTiO_3$, and $Sr_{1-y}Ca_yFeO_{3-x}$) oxides, have been reported for use as the active layer [2,3]. The mechanism for gas detection in these materials is based on reactions that occur at the sensor surface, resulting in a change in the concentration of adsorbed oxygen. Oxygen ions adsorb onto the material's surface, removing electrons from the bulk and creating a potential barrier that limits electron movement and conductivity. When reactive gases combine with this oxygen the height of the barrier is altered, changing conductivity. This change in conductivity is directly related to the composition of the gaseous environment allowing a quantitative determination of the gases present (under certain conditions) [4]. Metal oxide semiconductor sensors have proved to be sensitive to a large range of gases and studies have focused on understanding the relationship between sensor response and materials processing and chemistry, e.g., dopant level, synthesis and annealing

temperature. These parameters can have a profound effect on the materials chemistry and structure, which in turn dramatically affect the gas sensing properties of the sensor device [2]. Currently the potential of metal oxide semiconductor sensors has not been fully realised, with other types of sensors (e.g., electrochemical or those based on optical or photo-ionisation principles) still favored for many industrial applications. However, new materials and techniques continue to be developed to improve the abilities and properties of metal oxide gas sensors, and with recent advances in understanding of materials chemistry and synthetic techniques their intrinsically favourable properties, coupled with their relative low cost and potential for miniaturization and portability, should mean they become ever more important tools in environmental monitoring.

Development of synthetic methods for producing materials for use in metal oxide gas sensors has been a major focus in the field and many routes have been investigated including hydrothermal [5], sol-gel [6], solid-state chemical reaction [7], thermal evaporation [8], vapor-phase transport [9], RF sputtering [10] and molecular beam epitaxy [11]. Two common preparative routes are solid-state and sol-gel; solid-state reactions allow for relatively simple synthesis but for complex materials can lead to poor chemical homogeneity, whilst sol-gel reactions provide very good homogeneity and small particle size dispersion but the process can be difficult to control reproducibly. An alternative synthesis technique is chemical vapour deposition (CVD), which is a process for the deposition of films of various materials via chemical reactions of gaseous reactants in an activated environment (e.g., temperature, light or plasma). In general, a CVD system consists of three main components:

1. Precursor supply system
2. CVD reactor
3. Exhaust system.

The role of the precursor supply system is to generate precursors in the vapour phase and deliver them to the reactor, normally with the help of carrier gas, where the CVD reaction takes place. Typically, liquid precursors are used in order to generate sufficient vapour pressure when heated to intermediate temperature (<200 °C) with mixing of multiple precursor streams used to produce complex mixtures. Variants on this system such as liquid injection- and aerosol assisted-(AA)CVD [12] are typically used to introduce low volatility/solid precursors, with precursor evaporation only occurring inside the CVD reactor, although they also afford great opportunities in synthesizing doped or ternary/quaternary materials due to the relative ease of controlling stoichiometry through the precursor solution.

The reactor is where external energy is added to the system, in the form of heat, light or plasma, to initiate the deposition reaction(s). Deposition involves two principal types of reactions, homogenous and heterogeneous; homogeneous reactions occur exclusively in the gas phase whilst heterogeneous reactions occur between gas phase species and a solid substrate (although frequently involving an initial gas phase reaction resulting in the formation of reactive intermediate species). In the case of homogeneous reaction the precursor/intermediate species undergo further gas phase decomposition resulting in the formation of a powder and by-products. This powder is typically non-adherent and these reactions are undesirable in CVD (although in pyrolysis reactions the powder may be the target and collected via a powder capture system), whilst the by-products are removed from the reaction chamber through the exhaust system. In the case of heterogeneous reactions diffusion of the precursor/intermediate species occurs at an interfacial gas/solid boundary layer, forming nucleation sites on the solid substrate. Subsequent nucleation processes take place on the surface of substrate resulting in the deposition of solid material, and manipulation of the reaction conditions can be used to promote the formation of either planar films or nanostructures [13]. It is also worth noting that the nature of the heterogeneous reactions means that the materials are atomically mixed, and under well-controlled conditions are homogeneous in composition across the deposition area. Hence CVD offers several potential advantages over other synthesis processes for the preparation of gas sensing materials and sensors, which include:

- A single step for gas sensor processing which combines both materials synthesis and integration of the material with the sensor platform.
- Production of atomically mixed homogenous materials, including complex stoichiometries, with good reproducibility.
- Ability to influence crystal structure and surface morphology.

This article presents a review of recent research efforts and developments for the fabrication of metal-oxide gas sensors using chemical vapour deposition (CVD), presenting its potential advantages as a materials synthesis technique for gas sensors along with a discussion of their sensing performance. In considering the literature we have compiled tables of sensing data, however we note that these are only a qualitative comparison as the response of metal oxide semiconductors in general is dependent not only on the material properties but also on the conditions used to test these materials towards the analytes.

2. Gas Sensing Materials

2.1. Tungsten Oxide

Tungsten oxide, WO_3, is a wide-bandgap *n*-type semiconductor, with bandgaps reported in the range of approximately 2.6–3.2 eV dependent on crystallinity and oxygen deficiency. WO_3 crystals are generally formed by corner and edge sharing of WO_6 octahedra, with various crystal phases dependent on temperature; monoclinic II (ε-WO_3, < −43 °C) → triclinic (δ-WO_3, −43 ° C to 17 °C) → monoclinic I (γ-WO_3, 17 °C to 330 °C) → orthorhombic (β-WO_3, 330 ° C to 740 °C) → tetragonal (α-WO_3, > 740 °C). Tungsten oxide can also possess non-stoichiometric properties because its rhenium oxide-like lattice can withstand a considerable amount of oxygen deficiency. Some of the better known non-stoichiometric tungsten oxides are $W_{20}O_{58}$, $W_{18}O_{49}$ and $W_{24}O_{68}$ [14].

Vapour deposited WO_3 and WO_x have both been used for gas sensing. These materials are typically monoclinic or tetragonal phases with a variety of morphologies reported including films, particles and low dimensional structures, with the formation of nanostructures (NS) demonstrated below 600 °C for AACVD [15] and at 800 °C for hot filament CVD. The starting materials reported in the production of gas sensitive tungsten oxide include metallic W [16,17], WO_3 (powder, pellet) [18,19], WCl_6 [20], $W(OCl_4)$ [21], $W(CO)_6$ [22–24], or complexes such as $[W(OPh)_6]$ [25,26], $[NH_4][W_{12}O_{39}]$, $[NH_4]_{10}H_2[W_2O_7]_6$ or $[^nBu_4N]_2[W_{10}O_{32}]$ [27]. Most commonly planar films of vapour deposited tungsten oxide have been employed and integrated directly into ceramic- [20,21,26,27], silicon- [16,22,23,25] or polymer-based [28] gas sensing devices. The localized CVD of tungsten oxide nanostructures on Si-based microhotplates (Figure 1) via heating provided from the sensor platform itself, rather than from the reactor chamber, has also been demonstrated as a viable method for the fabrication of gas sensors based on tungsten oxide [23], which provides interesting new possibilities for sensor processing.

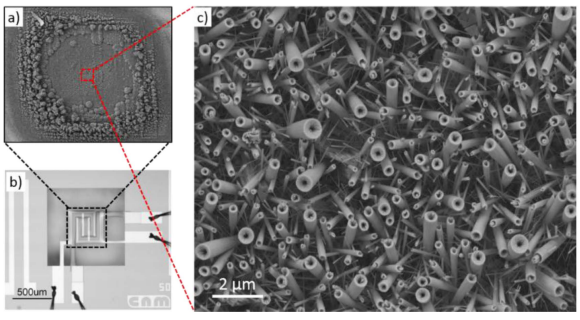

Figure 1. Scanning electron microscope images of WO_3 nanostructures grown at (**a**) low and (**b**,**c**) high magnification grown localized on microhotplates via AACVD. Adapted from [23].

As with other metal oxides, tungsten oxide deposited via CVD has been used in resistive mode, with demonstrated sensitivity to NO_2 [16,21,26], N_2O [17], C_2H_5OH [20,27], CO [23,25], NH_3 [18], H_2 [22], humidity [19] and aromatic compounds such as benzene [29] and toluene [30] (Table 1). The relative sensor response (R) to ppm concentrations (C) of CO, C_2H_5OH and NO_2 (Table 1) are plotted in Figure 2. This relative value (*i.e.*, Response/Concentration) was used as a quantitative factor to compare the sensitivity of the most common CVD-deposited tungsten oxide morphologies reported in the literature, although it is worth noting that strictly sensitivity is defined as the slope of the calibration curve (calibration curves were not available in most of the reports summarized in Table 1). It is apparent from Figure 2 that tungsten oxide has a notable sensitivity to NO_2 and this characteristic is generally observed for tungsten oxide making it a good candidate to selectively detect NO_2 in the presence of gases such as C_2H_5OH, CH_4, CO, NH_3, H_2, C_6H_6 and H_2S [21,24].

Table 1. Summary of the features and sensing properties reported for chemical vapour deposited tungsten oxide.

Prec.	CVD method	T_{dep} °C	Form	Features nm	Sensor type	T_{op} °C	ppm	Gas	R	t_{res} s	Ref.
$W(OCl_4)$	PE	-	film	-	Ω	200	10	NO_2	48	-	[21]
WCl_6	AP	625	film	3600^{T}	Ω	400	20	C_2H_5OH	8.5	-	[20]
$W(CO)_6$	LP	500	NPs	$140^{Ø}$	Ω	>450	5000	H_2	***	-	[22]
W	HF	-	NPs	$100^{Ø}$	Ω	50	1	NO_2	4701	-	[16]
WO_3	EB	-	NPs	$9^{Ø}$ 200^{T}	NS*	100	10	NH_3	-	-	[18]
W^{CMPLX}	AA	500	P	$1000^{Ø}$ $30{,}000^{T}$	Ω	550	20	C_2H_5OH	5.1	-	[27]
W	HF	800	NWs	-	Ω	450	1	N_2O	4.41	175	[17]
$W(OPh)_6$	AA^{EF}	-	NWs	–	Ω	250	0.8	NO_2	120	-	[26]
$W(CO)_6$	$AA^{L\circ c}$	580	NWs	$100–400^{Ø}$	Ω	375	80	CO	8	-	[23]
$W(OPh)_6$	AA	400	NWs	$60–120^{Ø}$ 7000^{L}	Ω	150	100	CO	5	-	[25]
$W(OPh)_6$	AA	400	NWs	$60–120^{Ø}$ 7000^{L}	Ω	200	1	C_6H_6	2	1114	[29]
$W(CO)_6$	AA	500	NWs	$50–100^{Ø}$ 11000^{L}	Ω	390	0.4	NO_2	250	-	[24]
$W(CO)_6$	AA	390	NWs	$50–100^{Ø}$ $10{,}000^{L}$	Ω	190 220	100 100	C_7H_8 C_2H_5OH	3 3.5	450 -	[30]
$WO_{2.9}$	CVD	400	NRs	$30–110^{Ø}$ 1000^{T}	O	RT	65**	H_2O	2.16	-	[19]

Prec: precursors, T_{dep}: temperature of deposition, T_{op}: operating temperature, t_{res}: response time, ppm: parts per millon, R = Ra/Rg (oxidative gas), R = Rg/Ra (reductive gas), ^{CMPLX}: $[^{n}Bu_4N]_2[W_{10}O_{32}]$, PE: plasma enhanced, AP: atmospheric pressure, LP: low pressure, HF: Hot Filament, EB: Electron Beam, AA: Aerosol assisted, ^{EF}: Electric field, $^{L\circ c}$: Localized, O: optical, Ω: resistive, NS: noise spectroscopy, *: gas sensing assisted by Blue-LED, **: % Relative humidity, ***: low response and not stable, NPs: nanoparticles, NWs: nanowires, NRs: nanorods, ^{Ø}: diameter, ^{T}: film thickness, L: length.

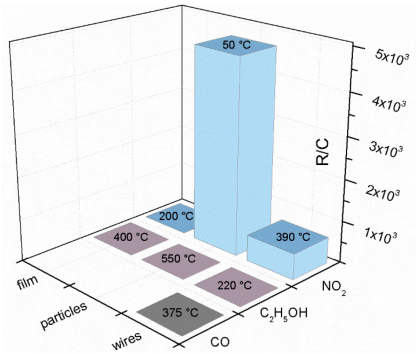

Figure 2. Relative sensor response (R) to ppm concentration (C) of NO_2, C_2H_5OH and CO against operating temperature for different tungsten oxide morphologies (based on the maximum response for the minimum concentration in Table 1 for each morphology/gas combination).

The properties of CVD have been used to enhance the performance of thin film tungsten oxide-based resistive sensors in several ways. For instance, the sensing properties to ethanol were improved by a change in microstructure that occurred by controlling film thickness in the range 6700 nm to 3600 nm. These changes produced a reduction in the baseline resistance of the sensors, with resistance decreasing with decreasing film thickness, with an attendant modification of the activation energy of conductance [20]. We note a similar study has demonstrated improved sensor performance in *thicker* films (30,000 nm) compared to thinner films (15,000 nm) [27], but it is likely that these results are influenced by the properties of the electrodes, specifically the electrode thickness, which need to have a similar thickness to that of the thin film sensor material in order to achieve optimum sensor performance [31]. For NP tungsten oxide, CVD has been used to control the size of NPs to improve sensor performance, with particles with sizes below 100 nm having better sensing properties to NO_2 regardless of processing parameters such as the oxygen pressure during CVD or the subsequent annealing temperature. This was attributed to the depletion layer extending throughout the material in small particles hence providing a larger conductivity change than for large particles that which are depleted only at the surface [16]. In addition, by manipulating CVD conditions to favour formation of networked nanowire mats rather than NPs the sensitivity of tungsten oxide to N_2O was improved by an order of magnitude compared to NP films (Figure 3). This was related to the higher surface-to-volume ratio of NS compared to NPs, although this study also highlights the need to use highly networked nanowires as opposed to (quasi) aligned nanowires for optimum gas sensing performance, as these behave similarly to single nanowire or parallel nanowire arrays [17]. Similar observations were also reported for gas microsensors based on tungsten oxide nanoparticles and nanowires grown via AACVD (Figure 3) [32].

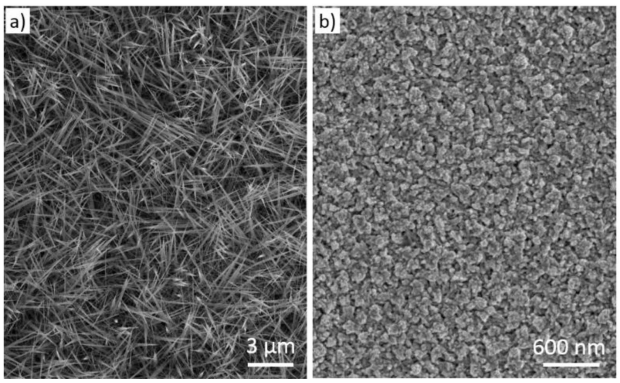

Figure 3. Scanning electron microscope images of (**a**) nanowire mat (**b**) NP films. Adapted from [32].

CVD has also been demonstrated to simplify sensor processing by providing direct integration of tungsten oxide sensor materials with the sensor platform. This has been demonstrated particularly for aerosol assisted CVD, which has shown the selective deposition of networked or quasi-aligned tungsten oxide NS on ceramic- [33], silicon- [32] and polymer-based platforms [28].

2.2. Zinc Oxide

Zinc oxide (ZnO) is a II-VI semiconductor with a wide direct band gap (3.37 eV), large exciton binding energy (60 meV), spontaneous polarization and piezoelectric constants which make it an attractive material for electronic, optoelectronic, energy generator and photocatalytic applications [34]. This material has been widely used for gas detection since the early 1960s, and it is still among the most reported metal oxide materials used for gas sensing. Most of the interesting functionalities of ZnO originate from its wurtzite crystal structure, which can be described as a number of alternating planes composed of tetrahedrally coordinated O^{2-} and Zn^{2+} ions, stacked along the *c*-axis. This crystal does

not possess inversion symmetry, having a large spontaneous polarization along the [0001] crystalline direction [34,35].

Metallic Zn [36–43] or diethylzinc (Et_2Zn) [44–47], both with O_2 as carrier (reactive) gas, have been used as precursors for the formation of ZnO via CVD, although other simple precursors such as zinc nitrate ($Zn(NO_3)_2$) [48] and organometallic complexes (e.g., Zn(II) ketoiminate) [49,50], have also been reported. ZnO films or NPs have been typically achieved at deposition temperatures between 350 and 450 °C, whereas NS of this material have been reported at deposition temperatures exceeding 450°C, either with or without the use of gold (catalytic) seeds to encourage NS formation. Similarly to tungsten oxide, CVD has been used to facilitate processing of sensors with the deposited zinc oxide often integrated directly onto planar ceramic- or silicon-based gas sensing devices, with the exception of structures in the form of wires which apparently have been exclusively used as single structures integrated into the device after a post-transfer process (*i.e.*, single wire sensors) (Table 2).

Table 2. Summary of the features and sensing properties reported for chemical vapour deposited zinc oxide.

Prec.	CVD method	T_{dep} °C	Form	Features nm	Sensor Type	T_{op} °C	ppm	gas	R	t_{res} s	Ref.
Et_2Zn	MO	-	Film	130^{FT}	Ω	300	1660	CO	1.6	-	[44]
Et_2Zn	PE	-	Film	500^{FT} 38^{CZ}	Ω +O	RT	200000	O_2	1.8	-	[45]
Zn^{CMPLX}	AA	450	Film	25^{CZ}	Ω	60	500	C_2H_5OH	2	10	[51]
Et_2Zn	MO	450	NPs	-	Ω	300	1000	CO	1.53	-	[46]
$Zn(OAc)_2$	AA	350	NPs	12^{CZ}	Ω	300	10000	DMA	1.7	240	[52]
Zn	CVD	550	NWs	$30000^{Ø}$	$Ω+O^{SNW}$	RT	200	C_2H_5OH	2	-	[36]
ZnO	CVD	-	NWs	$130^{Ø}$ 4000^{L}	$Ω+O^{SNW}$	200	1×10^6	CO	4	-	[53]
Zn	CVD	-	NWs	$80^{Ø}$ 3500^{L}	FET^{SNW}	-	400	CO	3	-	[37]
Zn	UHV	650	NWs	$100^{Ø}$	$Ω+O^{SNW}$	RT	100	H_2	1.35	3	[38]
Et_2Zn	MO	500	NRs	$100^{Ø}$	Ω	300	500	O_2	3.5	-	[47]
Zn	CVD	600	NRs	-	Ω+O	RT	2.5	O_3	1300	45	[39]
Zn	PE	-	NRs	$100^{Ø}$ 2000^{L}	Ω	400		CH_2O	100	-	[40]
Zn	CVD	700	HS	-	Ω	RT	250	CO	1.8	-	[41]
Zn	VT	700	HS	800^{TB} 150^{TC}	FET^{SNW}	200	1	NO_2	2	-	[42]
Zn^{CMPLX}	PE	300	HS		Ω	100	0.28	O_3	1000	-	[49]
Zn	VT	410	HS	$5000^{Ø}$	Ω	400	205	CH_2O	38	-	[43]
Zn^{CMPLX}	PE	300	HS		Ω	400	5000	H_2	14	-	[50]
$Zn(NO_3)_2$	C	1100	F	20000	$Ω^{SF}$	400	500	C_2H_5OH	15.3	-	[48]

Prec: precursors, T_{dep}: temperature of deposition, T_{op}: operating temperature, t_{res}: response time, ppm: parts per millon, R = Ra/Rg (oxidative gas), R = Rg/Ra (reductive gas), Et2Zn: Diethylzincm, ^{CMPLX}: complex Ω: resistive, O: optical, ^{SNW}: single nanowire configuration, ^{SF}: single flake, ^{FT}: film thickness, ^{Ø}: diameter, L: length, CZ: Crystallite size, ^{TC}: thickness of the combs, ^{TB}: thickness of the NBs, NWs: nanowires, NPs: nanoparticles, NRs: nanorods, HS: hierarchical structures, F: flake, DMA: Dimethylamine.

Chemical vapour deposited ZnO has shown sensitivity to gases such as CO [37,41,44,46,53], H_2 [38,46,50], C_2H_5OH [36,48], CH_2O [40,43], NO_2 [42,49], O_3 [39] and O_2 [45,47], working in resistive mode, although a few papers also report the use of ZnO in optical sensing [36,39,40,45,53]. The multifunctionality of ZnO has also allowed for the operation of sensors in an optical-resistive mode, in which adsorption of the gaseous molecules is induced via the use of UV light, which has been shown to favour the room temperature detection of O_3 [39] and CH_2O [40].

A comparison of the sensor response as a function of the gas concentrations in ppm (see Section 2.1 for details) for various CVD-deposited ZnO morphologies (Figure 4) suggests that ZnO NS provide improved sensor responses compared to thin films or particle-like films, which is consistent with the enhanced sensing properties attributed to high surface-to-volume-ratio materials. Whilst single

wire sensors based on ZnO have shown good response at room temperature, ZnO films comprised of NS such as flakes, rods, or belts grouped as mats, films or agglomerates may ultimately be more advantageous due to easier integration with sensor devices, whilst still possessing greater responses compared to particle-like planar films.

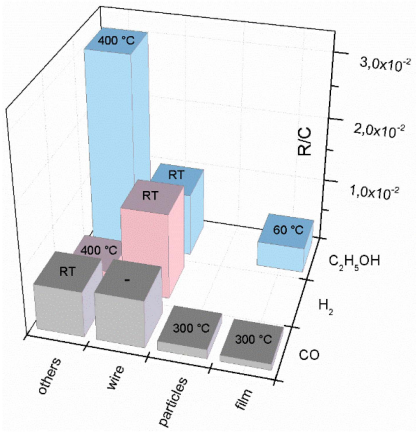

Figure 4. Relative sensor response (R) to ppm concentration (C) of H_2, C_2H_5OH and CO against operating temperature for different zinc oxide morphologies (based on the maximum response for the minimum concentration shown in Table 2 for each morphology/gas combination). Other structures: NR, NB, CL, flakes.

The ability to influence morphology in CVD deposited material has been exploited in a number of studies to improve the gas sensing performance of zinc oxide thin films, for instance by altering reaction conditions wurtzite structure films textured along the [001] direction were prepared with differing morphology. Optimal conditions for CO sensing were found when using columnar-like ZnO grains 130 nm thick, as opposed to grains growing laterally to the substrate sized 100, 110, and 160 nm [44].

Similarly improved sensor response to H_2 was recorded for single ZnO wires 100 nm in diameter as opposed to wires with diameters of 200 nm or 600 nm which showed lower responses (less than 10%) [38]. These results were attributed to the higher concentration of structural defects when the diameter of ZnO wires are decreased, and hence by targeting wires with smaller diameters sensor performance can be optimized. In addition, hexagonal ZnO wires with curved sides demonstrated superior ethanol sensing performance than similar wires with straight sides (Figure 5), which was attributed to higher surface-to-volume ratio of the curved side wires [36].

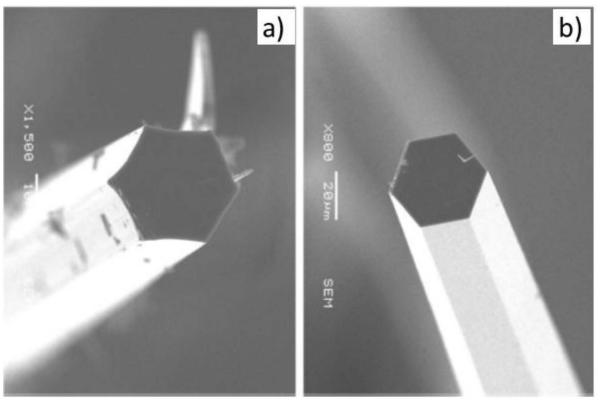

Figure 5. SEM images of a ZnO wire with curved (**a**) and straight (**b**) sides. Reprinted from [36] with permission from Springer.

A further demonstration of the use of CVD to manipulate morphology to improve sensor performance was obtained for hollow microspheres with nanorods grown on their outer surface formed *in-situ* during CVD reaction, which were found to possess more oxygen vacancies and surface sites compared to non-hierarchical structures due to structure-determined residual stress that promoted the adsorption of oxygen and electron trapping [43].

2.3. Tin Oxide

Tin oxide is an intrinsic *n*-type wide-bandgap (3.6–4.0 eV) semiconductor with applications in transparent conducting electrodes, antireflective coatings and gas sensors. The dual valence of tin, with tin preferably attaining oxidation states of +2 or +4, facilitates the variation of the surface oxygen composition and in turn the gas sensing properties of this material [54,55]. SnO_2 in its thick film form is one of the most used materials in current commercial resistive gas sensors, and is one of the most studied materials for gas sensing in the literature. Despite this the literature related to chemical vapour deposited SnO_2 for gas sensing is less reported than for other metal oxides.

Similarly to zinc and tungsten oxides, SnO_2 has been synthetized in the form of planar films, nanoparticles, nanowires and nanorods, with a strong dependence of the microstructure on the deposition temperature (Table 3), with films and particles reported at deposition temperatures below 400 °C and nanostructured SnO_2 obtained at temperatures exceeding 700 °C. The most common precursors for the synthesis of SnO_2 via CVD include metallic tin [56–58], salts ($SnCl_2$ and $SnCl_4$) [59–62], [$Sn(O^tBu)_4$] [55,63], and other less common precursors such as $Sn(NO_3)_4$ [64] and the complexes [$(CH_3(CH_2)_3CH(C_2H_5)CO_2)_2Sn$] and [Sn(18-crown-6)$Cl_4$] [65], with O_2 often used as a reactive carrier gas. SnO_2 films have often been tested without being integrated into traditional gas sensing devices whereas SnO_2 in the form of NPs and NS have been directly integrated with planar ceramic-platforms. In common with tungsten oxide the localized CVD of SnO_2 nanoparticles on Si-based microhotplates using the platforms microheaters has been shown to be a viable method for the integration of the sensing metal oxide with the sensor platform [64], whilst SnO_2 single nanowire sensors are typically integrated by means of a post-transfer process.

Table 3. Summary of the features and sensing properties reported for chemical vapour deposited tin oxide.

Prec.	CVD method	T_{dep}, °C	Form	Features, nm	Sensor type	T_{op} °C	ppm	gas	R	t_{res} s	Ref.
$SnCl_2.2H_2O$	CVD	-	Film	100^{T}	Ω	-	6	NO_2	1.2	-	[59]
TTB	MO	350	Film	50^{T}	Ω	RT	5	H_2S	1.1	-	[63]
$SnCl_4$	IBI	RT	Film	400^{T}	Ω	500	-	H_2	-	-	[60]
$SnCl_4$	ALD	250	Film	2.6^{T}	Ω	300	-	CO	43	-	[61]
TMH	LE	-	NPs	$\sim 15^{Ø}$	Ω	200	20	NO_2	77	160	[66,67]
$Sn(NO_3)_4$	Loc	375	NPs	-	Ω	-	200	CH_4O	5	-	[64]
T-crown	AA	400	NPs	$18–36^{Ø}$	Ω	300	10	NO_2	1.7	-	[65]
TEH	C	850	NPs	$1000^{Ø}$	Ω	300	500	C_2H_5OH	1075	31	[68]
$SnCl_2.2H_2O$	CVD	375	P	-	Ω	240	300	H_2	1.03	-	[62]
Sn	CVD	750	NWs	-	Ω		400	CO	3.9	10	[56]
Sn	CVD	800	NWs	$41^{Ø}$	Ω^{SNW}	300	500	NO_2	17	3	[57]
DBTA	PE	-	NRs	1200^{L} $45^{Øb}$-$10^{Ø}$	Ω^{SNW}	250	100	H_2	13	-	[69]
Sn	CVD	800	NWs	$60^{Ø}$ $20{,}000^{L}$	Ω	200	1	NO_2	90	8	[58]
TTB	CVD	700	Plates	$30–40^{T}$	Ω	250	100	C_2H_5OH	1.5	10	[55]

Prec: precursors, T_{dep}: temperature of deposition, T_{op}: operating temperature, t_{res}: response time, ppm: parts per millon, R=Ra/Rg (oxidative gas), R=Rg/Ra (reductive gas), TTB: Tin(IV)tert-butoxide, TEH: Tin(II)ethylhexanoate, T-crown: Sn(18-crown-6)Cl_4, TMH: Tetramethyltin, DBTA: dibutyltin diacetate, LE: laser enhanced, Loc: Localized, PE: plasma enhanced, C: combustion, IBI: ion beam induced, P: particles, NPs: nanoparticles, ^{Ø}: diameter, ^{Øb}: diameter at the base of nanostructure, ^{T}: film thickness, L: length, NWs: nanowires, NRs: nanorods. Ω: resistive, ^{SNW}: single nanowire configuration.

In general SnO_2 films deposited via CVD show sensitivity to NO_2 [57–59,65,66], CO [56,61], C_2H_5OH [55,68], H_2 [60,62,69], H_2S [63] and CH_3OH [64]. The relative sensor response (see Section 2.1 for details) in Figure 6 indicates similar performance for planar films and particles with a notable difference in sensors based on nanowires which show a high relative response to NO_2, although we note this could be related to the particular microtrenched transducing platform used or the use of Au catalyst seeds for the formation of the nanowires [58].

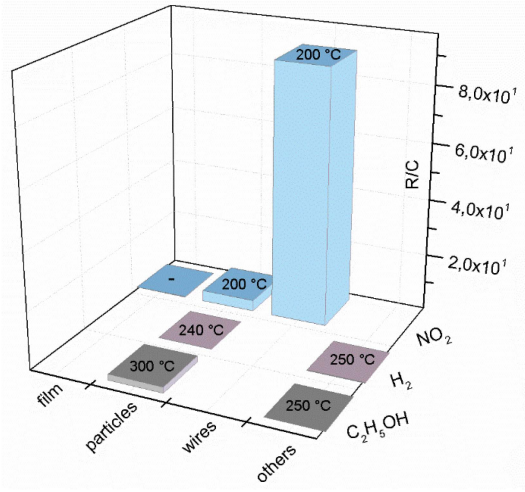

Figure 6. Relative sensor response (R) to ppm concentration (C) of H_2, C_2H_5OH and NO_2 against operating temperature for different tin oxide morphologies (based on the maximum response for the minimum concentration shown in Table for each morphology/gas combination). Other structures: NR and plates.

Laser-induced CVD (L-CVD) SnO_2 films with a grain-like (20 nm) surface showed enhanced sensing properties to NO_2 compared to SnO_2 films grown via an alternative rheotaxial growth and thermal oxidation (RGTO) method, with the magnitude of response doubled and the response time reduced. This was attributed to the smaller grains produced via L-CVD which were considered to improve gas diffusion through grains [66,67]. Similar observations were also noticed for SnO_2 grown via AACVD, indicating that grains with smaller size elongated in one direction increase the sensor response [65]. The positive influence of small grain-like SnO_2 surfaces for sensing reductive gases as H_2 compared to compact films was also noticed, and this was attributed to the higher degree of reduction to Sn^{2+} or Sn° species in grain-like SnO_2 surfaces, likely at the outermost surface layer of the grains where oxygen vacancies can be stabilized [60].

Atomic layer deposition (ALD), a technique which is related to CVD but allows atomic level control of film thickness, has also been used to examine the influence of SnO_2 film thickness on sensor performance. The response to CO was found to increase when increasing SnO_x ALD film thickness from 1.6 nm to 2.6 nm, whereas it decreased on further increasing film thickness from 2.6 nm to 5.9 nm [61]. The results were interpreted in terms of the Debye length and resistance for the films. The Debye length was comparable with the film thickness of 2.6 nm corresponding to the maximum responsivity for CO gas sensing. For film thicknesses >2.6 nm, the decrease in response was explained by a larger fraction of the film with thickness greater than the Debye length that was not affected by the O_2 and CO chemisorption. For film thicknesses <2.6 nm, the response decrease was attributed to the increasing resistance of the SnO_x ALD film. Similar observations were found for single nanowire sensors with diameter 40 nm, close to the depletion zone depth (13.4 nm) calculated for NO_2 adsorbed on SnO_2, which had higher response to NO_2 compared to wires with larger diameters (between 62 and 117 nm) [57]. This is similar to the results found previously for ZnO nanowires [38], although

the rationale provided is different (increased defect density for ZnO and Debye length for SnO_2). Thinner nanowires also showed an improved detection limit to NO_2 (Figure 7).

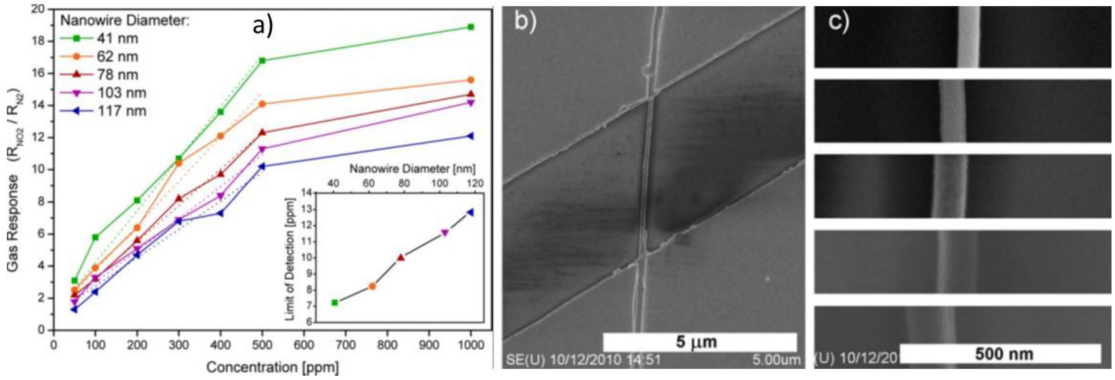

Figure 7. Gas responses of five single nanowire (SNW) sensors to various NO2 concentrations at 250 °C (**a**), and SEM images of a single nanowire connected to the electrodes (**b**) and and the NWs with different diameters (**c**) (from the bottom to the top: 117, 103, 78, 62, and 41 nm). Reprinted from [57] with permission from Elsevier.

2.4. Complex Oxides

The *p*-type semiconductor titanium-doped chromium oxide (CTO) $Cr_{2-x}Ti_xO_{3+y}$ ($0 \leqslant x \leqslant 0.4$) shows very good selectivity and sensitivity towards NH_3 and H_2S [70,71], with several techniques having been used to synthesize CTO gas sensing material including sol-gel [72–76], solid-state [77–79], solution [80,81] and CVD [82,83]. The synthesis of CTO powders, prepared via solid-state or sol-gel, and screen-printed onto an alumina sensor platform are the most widely used techniques but CTO has also been deposited using atmospheric pressure CVD (APCVD) using [CrO_2Cl_2] and [$TiCl_4$] or [Ti(O^ipr)$_4$] as metal precursors [83,84]. For APCVD deposited material the gas response against 80 pm of ethanol increased with reducing film thickness (Table 4), with thinner films also having higher ideal operating temperature, increasing from 500 to 575 °C on passing from 1500 to 500 nm film thickness. Comparison to 1500 nm thick screen-printed CTO sensors, using powder with an identical composition formed via solid-state synthesis, showed the screen-printed sensors had a better R/R_0 response towards ethanol (*ca.* 3–4) than an equivalent APCVD sensor (1.5), although film adhesion was better for the CVD material than the screen-printed one which was fragile and readily delaminated. The difference in sensitivity was attributed to microstructure, with the lower response against ethanol due to the high density/lack of microporosity in the microstructure. Subsequently electrostatic spray assisted vapour deposition (ESACVD) was used to manipulate microporosity when depositing $Cr_{1.8}T_{0.2}O_3$ onto silicon wafers [85,86]. An increase in film porosity was obtained by adding a low amount of polyvinyl alcohol and ethylene glycol to the precursor solution; Figure 11a,b shows the microstructure of CTO films obtained using 0.05 and 0.005 M respectively of precursor solution without addition of polymer whilst Figure 8c and 11d show the equivalent microstructure with addition of polymer. The sensors prepared with the addition of polymer exhibited an enhancement in the gas response towards 500 ppm of ammonia compared to those prepared without additive which was attributed to the increased porosity (30%–40% with polymer compared to 0%–20% without).

Cobalt(II,III) oxide, Co_3O_4, is a magnetic *p*-type semiconductor most often used as a heterogeneous catalyst, in Li-ion batteries or as a solid-state sensor [80,87–89]. CVD has been used to improve the sensor performance by homogenous doping with fluorine, with F-doped Co_3O_4 successfully grown at temperatures between 200 and 400 °C by plasma enhanced-chemical vapour deposition using single-source precursors, Co(dbm)$_2$ (where dbm = 1,3-Diphenyl-1,3-propanedione) and Co(hfa)$_2$TMEDA (where hfa = 1,1,1,5,5,5-hexafluoro-2,4-pentanedionate and TMEDA = N,N,N′,N′-tetramethylethylenediamine) respectively [90]. Sensors were tested against 100 ppm of

acetone at different operating temperatures and whilst undoped films exhibited a higher sensitivity when the operating temperature was 300 or 400 °C, F-doped Co_3O_4 operating at 200 °C showed the best response of all the tested sensors (Table 4). The addition of fluorine, which is reported to increase the carrier concentrations/mobility of *n*-type oxide semiconductors [91,92], unexpectedly produced a higher current response in the *p*-type Co_3O_4 at an operating temperature of 200 °C. The presence of fluorine was thought to increase the number of holes (h^+), the main *p*-type semiconductor charge carriers, by saturating dangling bonds at the surface of Co_3O_4 which otherwise would have trapped h^+ carriers and hence reduced conductivity [93].

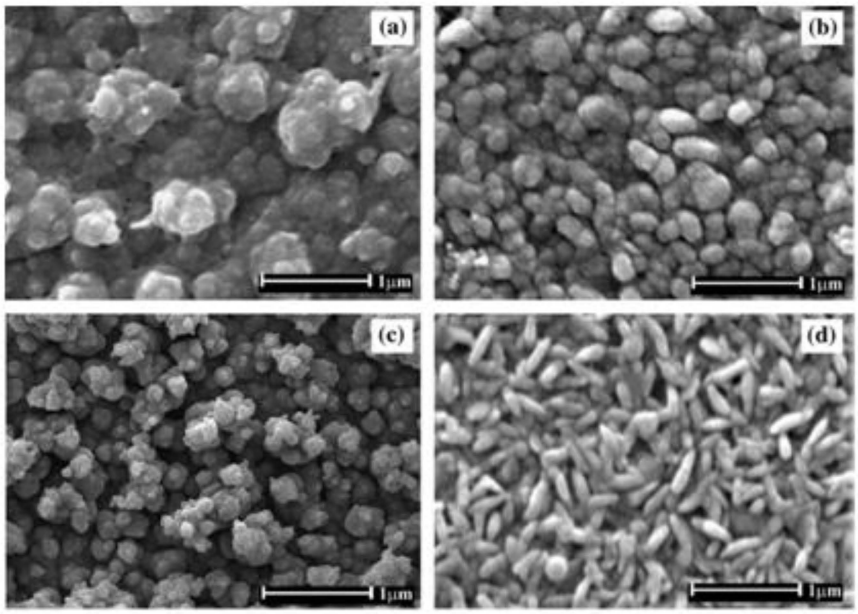

Figure 8. SEM photographs of $Cr_{1.8}Ti_{0.2}O_3$ films deposited at 650 -C from the different precursor without additive (**a**) 0.05 M, (**b**) 0.005 M, and with additive (**c**) 0.05 M, (**d**) 0.005 M. Reprinted from [85] with permission from Elsevier.

In_2O_3 is a widely used material in transparent conductors, in display panels and solar cell windows, in optical-antistatic coatings and it has also been used in gas sensing, with the typically low conductivity of In_2O_3 improved by doping it with zinc, titanium or tantalum [94,95]. CVD has been used to deposit mat-like Zn-doped In_2O_3 nanowires (NWs), at substrate temperatures between 400 and 550 °C, with the deposited Zn-In_2O_3 nanowires being 10–30 μm long with diameters between 50 and 300 nm (Figure 9). ZnO and In_2O_3 with graphite powder were used as sources.

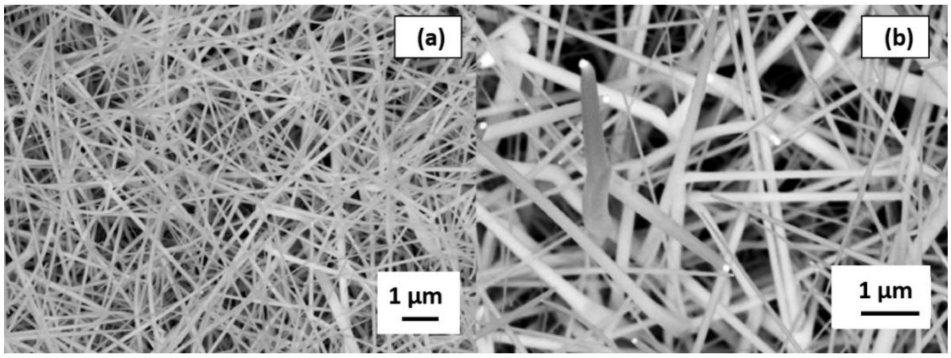

Figure 9. SEM images of Zn-In_2O3 NWs at (**a**) low and (**b**) high magnification. Reprinted from [94] with permission from Elsevier.

Gas response to CO was enhanced by addition of zinc as a dopant, with Ra/Rg increasing from 1.2 to 2.5 (Table 4). The response and recovery times were also dramatically improved (to 20 and 10 seconds respectively) with sensors based on undoped In_2O_3 not saturating within the period of test (500 seconds). Zinc-doped indium oxide proved to be selective against CO, being relatively more sensitive to CO than to NO_2 or NO. In_2O_3 has also been doped with tantalum or titanium via AACVD at 450°C using $InMe_3$ (where Me = methyl) and $M(NMe_2)_n$ (where M = Ti, n = 4; M = Ta, n = 5) as precursors [95]. Undoped indium oxide films were comprised of nanoparticles ~ 100 nm in diameter, with tantalum doping reducing particle size to ~80 nm but titanium doping increasing particle size to ~150 ± 10 nm (Figure 10).

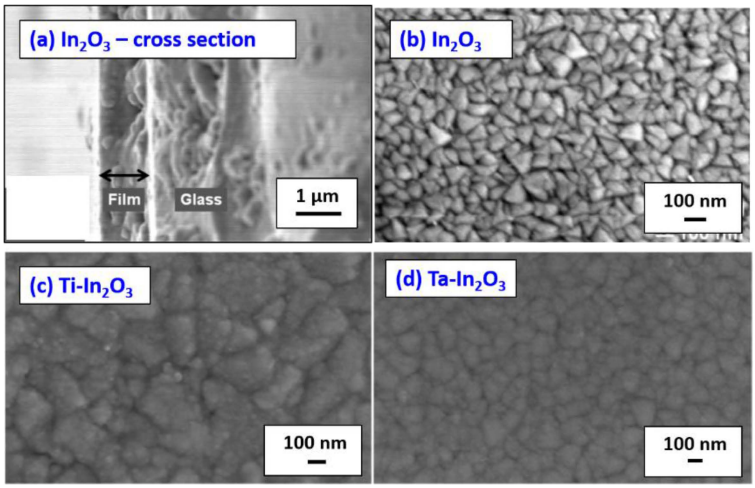

Figure 10. SEM images of (**a**) In_2O_3 cross section, (**b**) In_2O_3, (**c**) Ti- In_2O_3 and (**d**) Ta-In_2O_3. Reprinted from [95] with permission from American Chemical Society.

Table 4. Summary of the features and sensing properties reported for chemical vapour deposited complex metal oxides.

Material	Prec.	CVD Method	T_{dep} °C	FT nm	T_{op} °C	ppm	gas	R	Ref.
Co_3O_4:F	$Co(dpm)_2$ $Co(hfa)_2 \cdot$ TMEDA	PE	200 300 400		200	100	Acetone		[90]
Cr_2O_3:Ti	$Cr(acac)_3$ Ti-butoxide	AA	550	150-1000					[82]
Cr_2O_3:Ti	CrO_2Cl_2 $TiCl_4$	AP	400 475 550	500 1000 1500	400	80	CH_3CH_2OH	3.1 1.7 1.1	[83,84]
Cr_2O_3:Ti	Chromium acetate $Ti(acac)_2OiPr_2$	ESAVD	650		200 300400500	500	NH_3	1.05 1.18 1.22 1.46	[85,86]
In_2O_3:Ta	$InMe_3$ $Ta(NMe_2)_5$	AA	550	650	500	100 0.08	CH_3CH_2OH NO_2	16.9 3.01	[95]
In_2O_3:Ti	$InMe_3$ $Ti(NMe_2)_4$	AA	550	790	500	100 0.08	CH_3CH_2OH NO_2	2.62 1.80	[95]
In_2O_3:Zn	ZnO In_2O_3	CVD	400-550		RT	1-5	CO		[94]
SnO_2:In	$SnCl_4$ $InCl_3$	CVD	400	200	50-250	1000	H_2 Methanol CO	1.14 1.23 1.20	[96,97]

Prec: precursors, T_{dep}: temperature of deposition, T_{op}: operating temperature, ppm: parts per millon, R=Ra/Rg (oxidative gas), R=Rg/Ra (reductive gas), FT: film thickness, ES: Electrostatic spray assisted vapour deposition, PE: plasma enhanced, TMA: Trimethylamine, acac: cetylacetone, Me: methyl, TMEDA: tetramethylethylenediamine.

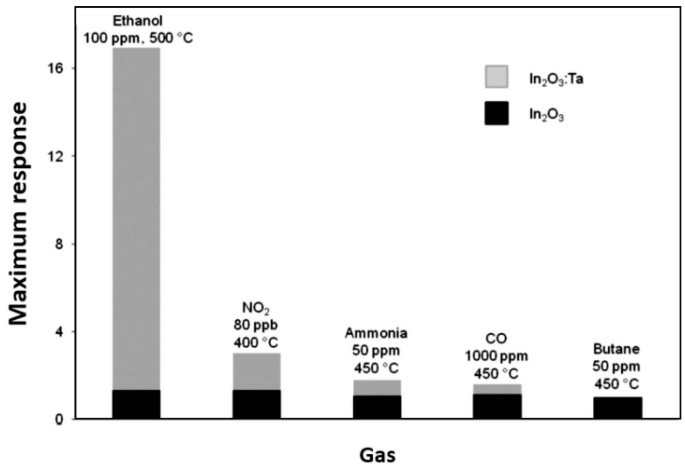

Figure 11. Maximum gas response of doped and undoped In_2O_3 against different gases at optimum operating temperature. Reprinted from [95] with permission from American Chemical Society.

Ta-In_2O_3 showed a much higher response to ethanol than either Ti-doped (~six times greater) or undoped (~sixteen times greater) In_2O_3 (Table 4), with the enhanced sensitivity ascribed to the decreased grain size and hence increased surface area. The response of Ta-In_2O_3 towards ethanol was particularly enhanced relative to the increase in sensitivity towards NO_2, NH_3, CO or butane where the greatest enhancement compared to an undoped sensor was double (Figure 11), suggesting there is also a chemical enhancement for ethanol sensing over and above the increase due to surface area. These results are in contrast to those obtained using Zn as the dopant which displayed particular enhancement towards CO (over NO_2) [94], indicating the potential to provide selectivity in In_2O_3 via use of different of dopant atoms.

3. Conclusions

Chemical vapour deposition has been used for synthesis of a wide variety of gas sensitive metal oxides. Planar thin films typically have poorer gas sensing performance compared to traditional screen printed equivalent, attributed to reduced porosity, but the ability to manipulate deposition conditions to alter microstructure, and/or promote formation of nanostructured materials, can mitigate reduced sensitivity. CVD is a highly promising technique for new materials synthesis due to its ability to homogenously form the complex doped and ternary/quaternary compositions which are likely to be at the heart of future advances in the field. However the real benefit of CVD is realised when considering lower power microsensor platforms, either alumina, silicon or polymer, where the ability to reproducibly integrate materials directly with the sensor platform provides an important process benefit compared to competing synthetic techniques. This advantage is likely to drive increased interest in the use of CVD for gas sensor materials over the next decade, and hence the current prospects for use of CVD in this field look excellent.

Acknowledgments: S.V. is supported by the SoMoPro II Programme, co-financed by the European Union and the South-Moravian Region, via Grant 4SGA8678. F.dM. is supported by UCL through its Impact Studentship Programme.

Conflicts of Interest: The authors declare no conflict of interest.

References

1. Yamazoe, N. Toward innovations of gas sensor technology. *Sens. Actuators B: Chem.* **2005**, *108*, 2–14. [CrossRef]
2. Korotcenkov, G. Metal oxides for solid-state gas sensors: What determines our choice? *Mater. Sci. Eng. B* **2007**, *139*, 1–23. [CrossRef]

3. Eranna, G.; Joshi, B.C.; Runthala, D.P.; Gupta, R.P. Oxide Materials for Development of Integrated Gas Sensors—A Comprehensive Review. *Crit. Rev. Solid State Mater. Sci.* **2004**, *29*, 111–188. [CrossRef]
4. Barsan, N.; Weimar, U. Conduction Model of Metal Oxide Gas Sensors. *J. Electroceramics* **2001**, *7*, 143–167. [CrossRef]
5. Wang, H.; Liang, J.; Fan, H.; Xi, B.; Zhang, M.; Xiong, S.; Zhu, Y.; Qian, Y. Synthesis and gas sensitivities of SnO2 nanorods and hollow microspheres. *J. Solid State Chem.* **2008**, *181*, 122–129. [CrossRef]
6. Siciliano, P. Preparation, characterisation and applications of thin films for gas sensors prepared by cheap chemical method. *Sens. Actuators B: Chem.* **2000**, *70*, 153–164. [CrossRef]
7. Zhi-Peng, S.; Lang, L.; Li, Z.; Dian-Zeng, J. Rapid synthesis of ZnO nano-rods by one-step, room-temperature, solid-state reaction and their gas-sensing properties. *Nanotechnology* **2006**, *17*, 2266.
8. Dai, Z.R.; Pan, Z.W.; Wang, Z.L. Novel Nanostructures of Functional Oxides Synthesized by Thermal Evaporation. *Adv. Funct. Mater.* **2003**, *13*, 9–24. [CrossRef]
9. Zhu, Z.; Chen, T.-L.; Gu, Y.; Warren, J.; Osgood, R.M. Zinc Oxide Nanowires Grown by Vapor-Phase Transport Using Selected Metal Catalysts: A Comparative Study. *Chem. Mater.* **2005**, *17*, 4227–4234. [CrossRef]
10. Choopun, S.; Hongsith, N.; Mangkorntong, P.; Mangkorntong, N. Zinc oxide nanobelts by RF sputtering for ethanol sensor. *Phys. E: Low-Dimens. Syst. Nanostructures* **2007**, *39*, 53–56. [CrossRef]
11. Heo, Y.W.; Varadarajan, V.; Kaufman, M.; Kim, K.; Norton, D.P.; Ren, F.; Fleming, P.H. Site-specific growth of Zno nanorods using catalysis-driven molecular-beam epitaxy. *Appl. Phys. Lett.* **2002**, *81*, 3046–3048. [CrossRef]
12. Marchand, P.; Hassan, I.A.; Parkin, I.P.; Carmalt, C.J. Aerosol-assisted delivery of precursors for chemical vapour deposition: Expanding the scope of CVD for materials fabrication. *Dalton Trans.* **2013**, *42*, 9406–9422. [CrossRef] [PubMed]
13. Ling, M.; Blackman, C. Growth mechanism of planar or nanorod structured tungsten oxide thin films deposited via aerosol assisted chemical vapour deposition (AACVD). *Phys. Status Solidi C* **2015**, *12*, 869–877. [CrossRef]
14. Zheng, H.; Ou, J.Z.; Strano, M.S.; Kaner, R.B.; Mitchell, A.; Kalantar-zadeh, K. Nanostructured Tungsten Oxide—Properties, Synthesis, and Applications. *Adv. Funct. Mater.* **2011**, *21*, 2175–2196. [CrossRef]
15. Annanouch, F.E.; Vallejos, S.; Stoycheva, T.; Blackman, C.; Llobet, E. Aerosol assisted chemical vapour deposition of gas-sensitive nanomaterials. *Thin Solid Films* **2013**, *548*, 703–709. [CrossRef]
16. Meng, D.; Yamazaki, T.; Shen, Y.; Liu, Z.; Kikuta, T. Preparation of WO3 nanoparticles and application to NO2 sensor. *Appl. Surface Sci.* **2009**, *256*, 1050–1053. [CrossRef]
17. Deb, B.; Desai, S.; Sumanasekera, G.U.; Sunkara, M.K. Gas sensing behaviour of mat-like networked tungsten oxide nanowire thin films. *Nanotechnology* **2007**, *18*, 285501. [CrossRef]
18. Tesfamichael, T. Electron Beam Evaporation of Tungsten Oxide Films for Gas Sensors. *Sens. J. IEEE* **2010**, *10*, 1796–1802. [CrossRef]
19. Zhang, J.; Zhang, W.; Yang, Z.; Yu, Z.; Zhang, X.; Chang, T.C.; Javey, A. Vertically aligned tungsten oxide nanorod film with enhanced performance in photoluminescence humidity sensing. *Sens. Actuators B: Chem.* **2014**, *202*, 708–713. [CrossRef]
20. Ashraf, S.; Blackman, C.S.; Naisbitt, S.C.; Parkin, I.P. The gas-sensing properties of WO 3− x thin films deposited via the atmospheric pressure chemical vapour deposition (APCVD) of WCl 6 with ethanol. *Meas. Sci. Technol.* **2008**, *19*, 025203. [CrossRef]
21. Tong, M.; Dai, G.; Wu, Y.; He, X.; Gao, D. WO3 thin film prepared by PECVD technique and its gas sensing properties to NO2. *J. Mater. Sci.* **2001**, *36*, 2535–2538. [CrossRef]
22. Davazoglou, D.; Georgouleas, K. Low Pressure Chemically Vapor Deposited WO 3 Thin Films for Integrated Gas Sensor Applications. *J. Electrochem. Soc.* **1998**, *145*, 1346–1350. [CrossRef]
23. Annanouch, F.E.; Gràcia, I.; Figueras, E.; Llobet, E.; Cané, C.; Vallejos, S. Localized aerosol-assisted CVD of nanomaterials for the fabrication of monolithic gas sensor microarrays. *Sens. Actuators B: Chem.* **2015**, *216*, 374–383. [CrossRef]
24. Annanouch, F.E.; Haddi, Z.; Vallejos, S.; Umek, P.; Guttmann, P.; Bittencourt, C.; Llobet, E. Aerosol-Assisted CVD-Grown WO3 Nanoneedles Decorated with Copper Oxide Nanoparticles for the Selective and Humidity-Resilient Detection of H2S. *ACS Appl. Mater. Interfaces* **2015**, *7*, 6842–6851. [CrossRef] [PubMed]

25. Vallejos, S.; Umek, P.; Stoycheva, T.; Annanouch, F.; Llobet, E.; Correig, X.; De Marco, P.; Bittencourt, C.; Blackman, C. Single-Step Deposition of Au- and Pt-Nanoparticle-Functionalized Tungsten Oxide Nanoneedles Synthesized Via Aerosol-Assisted CVD, and Used for Fabrication of Selective Gas Microsensor Arrays. *Adv. Funct. Mater.* **2013**, *23*, 1313–1322. [CrossRef]
26. Naik, A.J.T.; Bowman, C.; Panjwani, N.; Warwick, M.E.A.; Binions, R. Electric field assisted aerosol assisted chemical vapour deposition of nanostructured metal oxide thin films. *Thin Solid Films* **2013**, *544*, 452–456. [CrossRef]
27. Ashraf, S.; Blackman, C.S.; Palgrave, R.G.; Parkin, I.P. Aerosol-assisted chemical vapour deposition of WO3 thin films using polyoxometallate precursors and their gas sensing properties. *J. Mater. Chem.* **2007**, *17*, 1063–1070. [CrossRef]
28. Vallejos, S.; Gràcia, I.; Figueras, E.; Sánchez, J.; Mas, R.; Beldarrain, O.; Cané, C. Microfabrication of flexible gas sensing devices based on nanostructured semiconducting metal oxides. *Sens. Actuators A: Phys.* **2014**, *219*, 88–93. [CrossRef]
29. Vallejos, S.; Stoycheva, T.; Llobet, E.; Correig, X.; Umek, P.; Gracia, I.; Blackman, C. Benzene detection on nanostructured tungsten oxide MEMS based gas sensors. In Proceedings of the 2012 12th IEEE Conference on the Nanotechnology (IEEE-NANO), Birmingham, UK, 20–23 August 2012; pp. 1–5.
30. Vallejos, S.; Gràcia, I.; Figueras, E.; Cané, C. Nanoscale Heterostructures Based on Fe2O3@WO3-x Nanoneedles and Their Direct Integration into Flexible Transducing Platforms for Toluene Sensing. *ACS Appl. Mater. Interfaces* **2015**, *7*, 18638–18649. [CrossRef] [PubMed]
31. Boulmani, R.; Bendahan, M.; Lambert-Mauriat, C.; Gillet, M.; Aguir, K. Correlation between rf-sputtering parameters and WO3 sensor response towards ozone. *Sens. Actuators B: Chem.* **2007**, *125*, 622–627. [CrossRef]
32. Stoycheva, T.; Annanouch, F.E.; Gràcia, I.; Llobet, E.; Blackman, C.; Correig, X.; Vallejos, S. Micromachined gas sensors based on tungsten oxide nanoneedles directly integrated via aerosol assisted CVD. *Sens. Actuators B: Chem.* **2014**, *198*, 210–218. [CrossRef]
33. Stoycheva, T.; Vallejos, S.; Blackman, C.; Moniz, S.J.A.; Calderer, J.; Correig, X. Important considerations for effective gas sensors based on metal oxide nanoneedles films. *Sens. Actuators B: Chem.* **2012**, *161*, 406–413. [CrossRef]
34. Kozuka, Y.; Tsukazaki, A.; Kawasaki, M. Challenges and opportunities of ZnO-related single crystalline heterostructures. *Appl. Phys. Rev.* **2014**, *1*, 011303. [CrossRef]
35. Wang, Z.L. Nanostructures of zinc oxide. *Mater. Today* **2004**, *7*, 26–33. [CrossRef]
36. Zou, A.L.; Hu, L.Z.; Qiu, Y.; Cao, G.Y.; Yu, J.J.; Wang, L.N.; Zhang, H.Q.; Yin, B.; Xu, L.L. High performance of 1-D ZnO microwire with curve-side hexagon as ethanol gas sensor. *J. Mater. Sci. Mater. Electron.* **2015**, *26*, 4908–4912. [CrossRef]
37. Hung, S.C.; Woon, W.Y.; Lan, S.M.; Ren, F.; Pearton, S.J. Characteristics of carbon monoxide sensors made by polar and nonpolar zinc oxide nanowires gated AlGaN/GaN high electron mobility transistor. *Appl. Phys. Lett.* **2013**, *103*, 083506. [CrossRef]
38. Lupan, O.; Ursaki, V.V.; Chai, G.; Chow, L.; Emelchenko, G.A.; Tiginyanu, I.M.; Gruzintsev, A.N.; Redkin, A.N. Selective hydrogen gas nanosensor using individual ZnO nanowire with fast response at room temperature. *Sens. Actuators B: Chem.* **2010**, *144*, 56–66. [CrossRef]
39. Chien, F.S.-S.; Wang, C.-R.; Chan, Y.-L.; Lin, H.-L.; Chen, M.-H.; Wu, R.-J. Fast-response ozone sensor with ZnO nanorods grown by chemical vapor deposition. *Sens. Actuators B: Chem.* **2010**, *144*, 120–125. [CrossRef]
40. Han, N.; Hu, P.; Zuo, A.; Zhang, D.; Tian, Y.; Chen, Y. Photoluminescence investigation on the gas sensing property of ZnO nanorods prepared by plasma-enhanced CVD method. *Sens. Actuators B: Chem.* **2010**, *145*, 114–119. [CrossRef]
41. Zhang, H.-D.; Long, Y.-Z.; Li, Z.-J.; Sun, B. Fabrication of comb-like ZnO nanostructures for room-temperature CO gas sensing application. *Vacuum* **2014**, *101*, 113–117. [CrossRef]
42. Pan, X.; Liu, X.; Bermak, A.; Fan, Z. Self-Gating Effect Induced Large Performance Improvement of ZnO Nanocomb Gas Sensors. *ACS Nano* **2013**, *7*, 9318–9324. [CrossRef] [PubMed]
43. Zhang, D.; Wu, X.; Han, N.; Chen, Y. Chemical vapor deposition preparation of nanostructured ZnO particles and their gas-sensing properties. *J. Nanopart Res.* **2013**, *15*, 1–10. [CrossRef]
44. Pati, S.; Banerji, P.; Majumder, S.B. MOCVD grown ZnO thin film gas sensors: Influence of microstructure. *Sens. Actuators A: Phys.* **2014**, *213*, 52–58. [CrossRef]

45. Sanchez-Valencia, J.R.; Alcaire, M.; Romero-Gómez, P.; Macias-Montero, M.; Aparicio, F.J.; Borras, A.; Gonzalez-Elipe, A.R.; Barranco, A. Oxygen Optical Sensing in Gas and Liquids with Nanostructured ZnO Thin Films Based on Exciton Emission Detection. *J. Phys. Chem. C* **2014**, *118*, 9852–9859. [CrossRef]
46. Pati, S.; Maity, A.; Banerji, P.; Majumder, S.B. Qualitative and quantitative differentiation of gases using ZnO thin film gas sensors and pattern recognition analysis. *Analyst* **2014**, *139*, 1796–1800. [CrossRef] [PubMed]
47. Park, J.Y.; Choi, S.-W.; Kim, S.S. Fabrication of a Highly Sensitive Chemical Sensor Based on ZnO Nanorod Arrays. *Nanoscale Res. Lett.* **2010**, *5*, 353–359. [CrossRef] [PubMed]
48. Liu, Y.; Dong, J.; Hesketh, P.J.; Liu, M. Synthesis and gas sensing properties of ZnO single crystal flakes. *J. Mater. Chem.* **2005**, *15*, 2316–2320. [CrossRef]
49. Barreca, D.; Bekermann, D.; Comini, E.; Devi, A.; Fischer, R.A.; Gasparotto, A.; Maccato, C.; Sada, C.; Sberveglieri, G.; Tondello, E. Urchin-like ZnO nanorod arrays for gas sensing applications. *CrystEngComm* **2010**, *12*, 3419–3421. [CrossRef]
50. Barreca, D.; Bekermann, D.; Comini, E.; Devi, A.; Fischer, R.A.; Gasparotto, A.; Maccato, C.; Sberveglieri, G.; Tondello, E. 1D ZnO nano-assemblies by Plasma-CVD as chemical sensors for flammable and toxic gases. *Sens. Actuators B: Chem.* **2010**, *149*, 1–7. [CrossRef]
51. Hussain, M.; Mazhara, M.; Hussainb, T.; Khan, N.A. High efficiency ZnO nano sensor, fabrication and characterization. *JICS* **2010**, *7*, S59–S69. [CrossRef]
52. Roy, S.; Basu, S. Improved zinc oxide film for gas sensor applications. *Bull. Mater. Sci.* **2002**, *25*, 513–515. [CrossRef]
53. Kiasari, N.M.; Soltanian, S.; Gholamkhass, B.; Servati, P. Environmental Gas and Light Sensing Using ZnO Nanowires. *IEEE Trans. Nanotechnol.* **2014**, *13*, 368–374. [CrossRef]
54. Batzill, M.; Diebold, U. The surface and materials science of tin oxide. *Prog. Surface Sci.* **2005**, *79*, 47–154. [CrossRef]
55. Mathur, S.; Ganesan, R.; Grobelsek, I.; Shen, H.; Ruegamer, T.; Barth, S. Plasma-Assisted Modulation of Morphology and Composition in Tin Oxide Nanostructures for Sensing Applications. *Adv. Eng. Mater.* **2007**, *9*, 658–663. [CrossRef]
56. Trung, D.D.; Hoa, N.D.; Tong, P.V.; Duy, N.V.; Dao, T.D.; Chung, H.V.; Nagao, T.; Hieu, N.V. Effective decoration of Pd nanoparticles on the surface of SnO2 nanowires for enhancement of CO gas-sensing performance. *J. Hazard. Mater.* **2014**, *265*, 124–132. [CrossRef] [PubMed]
57. Tonezzer, M.; Hieu, N.V. Size-dependent response of single-nanowire gas sensors. *Sens. Actuators B: Chem.* **2012**, *163*, 146–152. [CrossRef]
58. Jung, T.-H.; Kwon, S.-I.; Park, J.-H.; Lim, D.-G.; Choi, Y.-J.; Park, J.-G. SnO2 nanowires bridged across trenched electrodes and their gas-sensing characteristics. *Appl. Phys. A* **2008**, *91*, 707–710. [CrossRef]
59. Bolotov, V.V.; Roslikov, V.E.; Roslikova, E.A.; Ivlev, K.E.; Knyazev, E.V.; Davletkildeev, N. A Formation of two-layer composite-on-insulator structures based on porous silicon and SnO x. Study of their electrical and gas-sensing properties. *Semiconductors* **2014**, *48*, 397–401. [CrossRef]
60. Jiménez, V.M.; Espinós, J.P.; González-Elipe, A.R. Effect of texture and annealing treatments in SnO2 and Pd/SnO2 gas sensor materials. *Sens. Actuators B: Chem.* **1999**, *61*, 23–32. [CrossRef]
61. Du, X.; George, S.M. Thickness dependence of sensor response for CO gas sensing by tin oxide films grown using atomic layer deposition. *Sens. Actuators B: Chem.* **2008**, *135*, 152–160. [CrossRef]
62. Ansari, S.G.; Gosavi, S.W.; Gangal, S.A.; Karekar, R.N.; Aiyer, R.C. Characterization of SnO2-based H2 gas sensors fabricated by different deposition techniques. *J. Mater. Sci.: Mater. Electron.* **1997**, *8*, 23–27.
63. Brown, J.R.; Haycock, P.W.; Smith, L.M.; Jones, A.C.; Williams, E.W. Response behaviour of tin oxide thin film gas sensors grown by MOCVD. *Sens. Actuators B: Chem.* **2000**, *63*, 109–114. [CrossRef]
64. Benkstein, K.; Martinez, C.; Li, G.; Meier, D.; Montgomery, C.; Semancik, S. Integration of nanostructured materials with MEMS microhotplate platforms to enhance chemical sensor performance. *J. Nanopart Res.* **2006**, *8*, 809–822. [CrossRef]
65. Stoycheva, T.T.; Vallejos, S.; Pavelko, R.G.; Popov, V.S.; Sevastyanov, V.G.; Correig, X. Aerosol-Assisted CVD of SnO2 Thin Films for Gas-Sensor Applications. *Chem. Vapor Depos.* **2011**, *17*, 247–252. [CrossRef]
66. Kwoka, M.; Ottaviano, L.; Szuber, J. Comparative analysis of physico-chemical and gas sensing characteristics of two different forms of SnO2 films. *Appl. Surface Sci.* **2015**, *326*, 27–31. [CrossRef]
67. Larciprete, R.; Borsella, E.; De Padova, P.; Perfetti, P.; Faglia, G.; Sberveglieri, G. Organotin films deposited by laser-induced CVD as active layers in chemical gas sensors. *Thin Solid Films* **1998**, *323*, 291–295. [CrossRef]

68. Liu, Y.; Koep, E.; Liu, M. A Highly Sensitive and Fast-Responding SnO2 Sensor Fabricated by Combustion Chemical Vapor Deposition. *Chem. Mater.* **2005**, *17*, 3997–4000. [CrossRef]
69. Hui, H.; Lee, Y.C.; Tan, O.K.; Zhou, W.; Peng, N.; Zhang, Q. High sensitivity SnO 2 single-nanorod sensors for the detection of H 2 gas at low temperature. *Nanotechnology* **2009**, *20*, 115501.
70. Moseley, P.T.; Williams, D.E. A selective ammonia sensor. *Sens. Actuators B: Chem.* **1990**, *1*, 113–115. [CrossRef]
71. Dawson, D.H.; Henshaw, G.S.; Williams, D.E. Description and characterization of a hydrogen sulfide gas sensor based on $Cr_{2-y}Ti_yO_{3+x}$. *Sens. Actuators B: Chem.* **1995**, *26*, 76–80. [CrossRef]
72. Pokhrel, S.; Li, X.; Huo, L.; Zhao, H.; Cheng, X. Investigation and characterization of radio frequency sputtered Cr1.8Ti0.2O3−δ thin films derived by citrate, sol–gel and solid state routes. *Thin Solid Films* **2007**, *515*, 7053–7058. [CrossRef]
73. Pokhrel, S.; Huo, L.; Zhao, H.; Gao, S. Sol–gel derived polycrystalline Cr1.8Ti0.2O3 thick films for alcohols sensing application. *Sens. Actuators B: Chem.* **2007**, *120*, 560–567. [CrossRef]
74. Nartowski, A.M.; Atkinson, A. Sol-Gel Synthesis of Sub-Micron Titanium-Doped Chromia Powders for Gas Sensing. *J. Sol-Gel. Sci. Technol.* **2003**, *26*, 793–797. [CrossRef]
75. Neri, G.; Bonavita, A.; Rizzo, G.; Galvagno, S. Low temperature sol-gel synthesis and humidity sensing properties of Cr2−xTixO3. *J. Eur. Ceramic Soc.* **2004**, *24*, 1435–1438. [CrossRef]
76. Chabanis, G.; Parkin, I.P.; Williams, D.E. Microspheres of the gas sensor material Cr2-xTixO3 prepared by the sol-emulsion-gel route. *J. Mater. Chem.* **2001**, *11*, 1651–1655. [CrossRef]
77. Niemeyer, D.; Williams, D.E.; Smith, P.; Pratt, K.F.E.; Slater, B.; Catlow, C.R.A.; Stoneham, A.M. Experimental and computational study of the gas-sensor behaviour and surface chemistry of the solid-solution Cr2-xTixO3 (x ⩽0.5). *J. Mater. Chem.* **2002**, *12*, 667–675. [CrossRef]
78. Peter, C.; Kneer, J.; Schmitt, K.; Eberhardt, A.; Wöllenstein, J. Preparation, material analysis, and morphology of Cr2-xTi xO3+z for gas sensors. *Phys. Status Solidi (A) Appl. Mater. Sci.* **2013**, *210*, 403–407. [CrossRef]
79. Jayaraman, V.; Gnanasekar, K.I.; Prabhu, E.; Gnanasekaran, T.; Periaswami, G. Preparation and characterisation of Cr2−xTixO3+δ and its sensor properties. *Sens. Actuators B: Chem.* **1999**, *55*, 175–179. [CrossRef]
80. Li, C.C.; Yin, X.M.; Wang, T.H.; Zeng, H.C. Morphogenesis of Highly Uniform CoCO3 Submicrometer Crystals and Their Conversion to Mesoporous Co3O4 for Gas-Sensing Applications. *Chem. Mater.* **2009**, *21*, 4984–4992. [CrossRef]
81. Pokhrel, S.; Ming, Y.; Huo, L.; Zhao, H.; Gao, S. Cr2-xTixO3 (x ⩽ 0.5) as CH3COCH3 sensitive resistors. *Sens. Actuators, B: Chem.* **2007**, *125*, 550–555. [CrossRef]
82. Conde-Gallardo, A.; Cruz-Orea, A.; Zelaya-Angel, O.; Bartolo-Pèrez, P. Electrical and optical properties of Cr2-xTixO 3 thin films. *J. Phys. D: Appl. Phys.* **2008**, *41*, 1–6. [CrossRef]
83. Shaw, G.A.; Parkin, I.P.; Williams, D.E. Atmospheric pressure chemical vapour deposition of Cr2-xTixO3 (CTO) thin films ([less-than-or-equal]3 [small micro]m) on to gas sensing substrates. *J. Mater. Chem.* **2003**, *13*, 2957–2962. [CrossRef]
84. Shaw, G.A.; Pratt, K.F.E.; Parkin, I.P.; Williams, D.E. Gas sensing properties of thin film (⩽3 μm) Cr2−xTixO3 (CTO) prepared by atmospheric pressure chemical vapour deposition (APCVD), compared with that prepared by thick film screen-printing. *Sens. Actuators B: Chem.* **2005**, *104*, 151–162. [CrossRef]
85. Du, J.; Wu, Y.; Choy, K.-L. Controlled synthesis of gas sensing Cr2−xTixO3 films by electrostatic spray assisted vapour deposition and their structural characterisation. *Thin Solid Films* **2006**, *497*, 42–47. [CrossRef]
86. Du, J.; Wu, Y.; Choy, K.-L.; Shipway, P.H. Structure, properties and gas sensing behavior of Cr2 − xTixO3 films fabricated by electrostatic spray assisted vapour deposition. *Thin Solid Films* **2010**, *519*, 1293–1299. [CrossRef]
87. Li, W.Y.; Xu, L.N.; Chen, J. Co3O4 Nanomaterials in Lithium-Ion Batteries and Gas Sensors. *Adv. Funct. Mater.* **2005**, *15*, 851–857. [CrossRef]
88. Choi, K.-I.; Kim, H.-R.; Kim, K.-M.; Liu, D.; Cao, G.; Lee, J.-H. C2H5OH sensing characteristics of various Co3O4 nanostructures prepared by solvothermal reaction. *Sens. Actuators B: Chem.* **2010**, *146*, 183–189. [CrossRef]
89. Jagadeesh, R.V.; Junge, H.; Pohl, M.-M.; Radnik, J.; Brückner, A.; Beller, M. Selective Oxidation of Alcohols to Esters Using Heterogeneous Co3O4–N@C Catalysts under Mild Conditions. *J. Am. Chem. Soc.* **2013**, *135*, 10776–10782. [CrossRef] [PubMed]

90. Barreca, D.; Bekermann, D.; Comini, E.; Devi, A.; Fischer, R.A.; Gasparotto, A.; Gavagnin, M.; Maccato, C.; Sada, C.; Sberveglieri, G.; *et al.* Plasma enhanced-CVD of undoped and fluorine-doped Co3O4 nanosystems for novel gas sensors. *Sens. Actuators B: Chem.* **2011**, *160*, 79–86. [CrossRef]
91. Ghosh, P.K.; Das, S.; Kundoo, S.; Chattopadhyay, K.K. Effect of Fluorine Doping on Semiconductor to Metal-Like Transition and Optical Properties of Cadmium Oxide Thin Films Deposited by Sol–Gel Process. *J. Sol-Gel. Sci. Technol.* **2005**, *34*, 173–179. [CrossRef]
92. Jinling, Y.; Jingkui, L.; Duo, J.; Shi, Y.; Weihua, T.; Guanghui, R. The influence of fluorine on the structures and properties of Pr2-xSrxCuO4-y (X = 0.0, 0.4, 1.0). *J. Phys.: Condens. Matter* **1997**, *9*, 1249.
93. Liu, B.; Gu, M.; Liu, X.; Huang, S.; Ni, C. First-principles study of fluorine-doped zinc oxide. *Appl. Phys. Lett.* **2010**, *97*, 122101. [CrossRef]
94. Singh, N.; Yan, C.; Lee, P.S. Room temperature CO gas sensing using Zn-doped In2O3 single nanowire field effect transistors. *Sens. Actuators B: Chem.* **2010**, *150*, 19–24. [CrossRef]
95. Bloor, L.G.; Manzi, J.; Binions, R.; Parkin, I.P.; Pugh, D.; Afonja, A.; Blackman, C.S.; Sathasivam, S.; Carmalt, C.J. Tantalum and Titanium doped In2O3 Thin Films by Aerosol-Assisted Chemical Vapor Deposition and their Gas Sensing Properties. *Chem. Mater.* **2012**, *24*, 2864–2871. [CrossRef]
96. Salehi, A.; Gholizade, M. Gas-sensing properties of indium-doped SnO2 thin films with variations in indium concentration. *Sens. Actuators B: Chem.* **2003**, *89*, 173–179. [CrossRef]
97. Salehi, A. Selectivity enhancement of indium-doped SnO2 gas sensors. *Thin Solid Films* **2002**, *416*, 260–263. [CrossRef]